# A Comprehensive Study on the Full Series of Alkali-Metal Selenocyanates $A^{I}$[SeCN] ($A^{I}$ = Li–Cs)

Alena Shlyaykher,[a] Marvin Ehmann,[a] Antti J. Karttunen,[b] and Frank Tambornino*[a]

**Abstract:** The full series of quasibinary alkali-metal selenocyanates was synthesized either by oxidation of the respective cyanides ($A$ = Li–Rb) or by metathesis ($A$ = Cs). For Li[SeCN] only ball-milling and subsequent annealing led to the isolation of the quasibinary selenocyanate. Their structures were refined from single-crystal and powder X-ray data. The respective solid-state IR and Raman spectra were interpreted with the aid of solid-state quantum-mechanical calculations and DSC-TGA measurements allowed for extraction of melting points. Only for Li[SeCN] a possible phase transition was observed that is discussed on the basis of VT-PXRD experiments. It is also the only quasibinary selenocyanate to form a hydrate (Li[SeCN]·2$H_2O$).

## Introduction

Chalcogenocyanates are archetypical pseudohalide anions with the general formula $Ch$CN$^-$ ($Ch$ = chalcogen). Of the potential six candidates (including Po and Lv), only the lightest four homologues have been synthesized so far: Cyanate (OCN$^-$), thiocyanate (SCN$^-$), selenocyanate (SeCN$^-$), and tellurocyanate (TeCN$^-$). Especially the chemistry of the cyanate and thiocyanate anions has been researched extensively and features in introductory and general chemistry textbooks. Due to their stability, ease of handling and ready availability, they have been widely used in coordination and organic chemistry. In contrast, selenocyanates and tellurocyanates are less stable and handling of these anions on air results in decomposition and deposition of elemental selenium and tellurium, respectively.

Fusion of potassium hexacyanoferrate(II) with sulfur had been shown to yield potassium thiocyanate. Consequently, reaction with the by that time new element–selenium–led to the synthesis of K[SeCN], probably the first selenocyanate containing compound, albeit with low yields.[1] Showing that the selenocyanate anion was in principle stable, the synthesis of K[SeCN] by oxidation from readily available KCN with Se was soon thereafter developed, proceeding in aqueous[2] and non-aqueous[3] solvents, as well as in melt,[4] yielding mostly pure product. Its crystal structure was studied decades later, confirming the linear structure of the anion.[5] Nowadays, K[SeCN] is commercially available and the selenocyanate starting material of choice for inorganic and organic chemists. The heavier tellurocyanate was first synthesized in 1968 and is, probably owing to its instability, the least studied of all chalcogenocyanates.[6,7]

Up until now, research on selenocyanates has been focusing on its use as ligand in complex compounds. All chalcogenocyanates are potentially ambidentate and will form N- or $Ch$-bonded complexes depending on the metal ion. Additionally, they also exhibit a range of bridging modes which has been used in the construction of metal–organic frameworks.[8–10] In organic chemistry, both the R–Se–C≡N and R–N=C=Se forms are known. Especially substances comprising the latter motif have received considerable attention as key intermediates towards the synthesis of Se-containing heterocycles. Such compounds are potential chemotherapeutic agents against cancer or infection diseases.[11]

Considering the historical and recent interest in (iso) selenocyanates it is all the more surprising how little is known about the simple quasibinary salts of the selenocyanate anion. While reports on the syntheses of Na[SeCN][3] and Cs[SeCN][12,13] can be found in literature, their crystal structures have not been reported. In fact, the only other reported crystal structure of a quasibinary selenocyanate is that of $Hg(SeCN)_2$,[14] which was reported alongside the homoleptic complexes $M_2$[$Hg(SeCN)_4$] ($M$ = K, Cs).[14]

In this contribution we present the full series of alkali-metal selenocyanates. Their syntheses, crystal structures, and thermal behaviors are discussed alongside vibrational spectroscopy (IR, Raman) which is corroborated by solid-state quantum mechanical calculations.

[a] A. Shlyaykher, M. Ehmann, Dr. F. Tambornino
Fachbereich Chemie and Wissenschaftlichen Zentrum für Materialwissenschaften (WZMW)
Philipps-Universität Marburg
Hans-Meerwein-Strasse 4, 35043 Marburg (Germany)
E-mail: frank.tambornino@chemie.uni-marburg.de

[b] Dr. A. J. Karttunen
Department of Chemistry and Materials Science
Aalto University
Kemistintie 1, 02150 Espoo (Finland)

Supporting information for this article is available on the WWW under https://doi.org/10.1002/chem.202102058

## Results and Discussion

### Syntheses

K[SeCN] is easily synthesized by oxidizing KCN with grey selenium, as has been reported before.[15] The starting materials are combined and refluxed in dry ethanol yielding a solution of K[SeCN] alongside insolubles for example surplus selenium or common impurities of KCN. If freshly precipitated red selenium is used instead, the reaction proceeds in solution at r.t. within minutes. Filtration and concentration of the resulting solution under reduced pressure affords K[SeCN] as an off-white powder in 98% isolated yield containing single crystals suitable for XRD.

Na[SeCN] is obtained similarly from NaCN and is also obtained in very good yields up to 99% as an off-white powder. Crystals suitable for SC-XRD were prepared by dissolution of 3.5 g Na[SeCN] in 1 ml degassed water at r.t. and subsequent slow evaporation of the solvent in a stream of argon.

Synthesis of Cs[SeCN] via salt metathesis reaction starting from CsCl has been reported and was replicated by us in good yields up to 75%. Attempted synthesis of Rb[SeCN] from K[SeCN] and RbCl resulted in incomplete metathesis reaction and formation of $K_xRb_{1-x}$[SeCN] with $x = 0.1–0.3$. Pure samples of Rb[SeCN] in good yields were obtained by similar conditions as applied for the syntheses of Na[SeCN] and K[SeCN].

The synthesis of Li[SeCN] was somewhat more challenging as the identification of a suitable solvent for salt metathesis was not straightforward. Reactions starting from K[SeCN] and LiCl in acetonitrile proceeded under formation of KCl (identified by PXRD) indicating a successful metathesis reaction. However, upon concentrating the solution under reduced pressure, a gloopy liquid was obtained which solidifies around 5 °C. $^{13}$C- and $^{77}$Se NMR spectroscopy showed signals for selenocyanate alongside larger amounts of solvent and SC-XRD indicated the formation of [Li(NCMe)$_3$(SeCN)]. Not unsurprisingly, coordinated acetonitrile could not be removed under reduced pressure. Application of elevated temperatures led to decomposition of the material under deposition of red Se. Salt metathesis reactions in other solvents had similar outcomes.

Oxidation of LiCN with grey or red selenium performed in various solvents suffered from similar formation of solvated compounds (e.g. Li[SeCN]·2H$_2$O, see below) which led us to explore solvent-free synthetic methods. Mechanochemical synthesis of Li[SeCN] in a ball-mill (from LiCN and grey selenium) allowed isolation of a grey, initially X-ray amorphous powder after only 5 minutes. $^{13}$C- and $^{77}$Se NMR alongside vibrational spectroscopy indicated absence of cyanide and formation of the selenocyanate anion. An endothermic signal in DSC-TGA measurements at 228 °C was accompanied by steady loss of mass over time and thus assigned to the melting point coinciding with a high vapor pressure. Heating a sample in fused borosilicate glass ampoules to 250 °C with subsequent slow cooling to r.t. resulted in formation of crystal needles several millimeters long (identified as Li[SeCN] by SC-XRD) alongside minor amounts of a grey powder (identified as Li$_2$Se by PXRD).

### Crystal structures of Li[SeCN] and Na[SeCN]

The crystal structures of Li[SeCN] and Na[SeCN] are isotypical in the orthorhombic system with space-group *Pnma* (no. 62, Li[SeCN]: $a = 7.8873(4)$, $b = 6.2442(4)$, $c = 5.4941(3)$ Å; Na[SeCN]: $a = 8.1745(4)$, $b = 7.0647(3)$, $c = 5.7171(3)$ Å) with 4 formula units in the unit cell (see Table S1 for details on data collection and structure refinement). Phase purity was confirmed by PXRD (for Li[SeCN] small amounts of Li$_2$Se were identified as side phase) and subsequent Rietveld refinement confirmed the model within small margins (see Table S3 and Figures S1 & S2). The structures do not correspond to a known structure type.

Cations occupy the Wyckoff position 4*b* (site symmetry −1) and they are surrounded by six $SeCN^-$ anions occupying position 4*c* (site symmetry *.m.*) in the form of a clinched octahedron. Four $SeCN^-$ anions coordinate with their selenium ($d_{(Li–Se)} = 2.8316(4)$ and 2.9186(4) Å, $d_{(Na–Se)} = 3.0457(1)$ and 3.0744(2) Å) two with their nitrogen terminus ($d_{(Li–N)} = 2.143(3)$, $d_{(Na–N)} = 2.4635(8)$ Å) as shown in Figure 1a, leading to CN = 6.

In the extended crystal structure the octahedra share faces thus forming columns along [010] (see Figure 1b). The columns exhibit rod group symmetry $\not{1}_b$ 1 $2_1/m$ 1 (no. 12) and its lattice periodicity is the *b* axis of the parent space-group. The rods

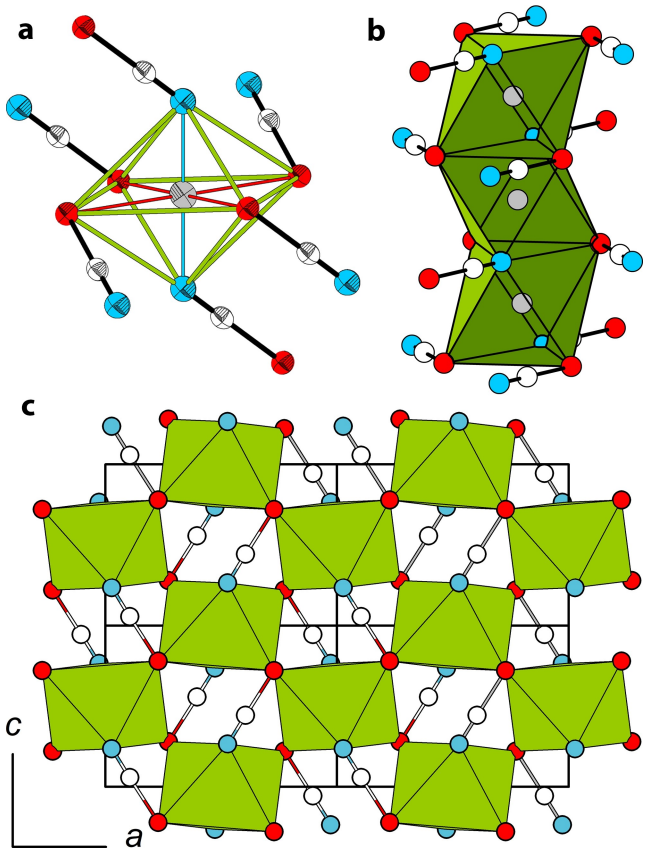


**Figure 1.** The crystal structure of Li[SeCN] (Na[SeCN] crystallizes isotypically). a) Coordination around the cation in the form of a clinched octahedron. b) Stack of octahedra with rod group symmetry $\not{1}_b$ 1 $2_1/m$ 1. c) 2×1×2 supercell emphasizing the distorted pseudohexagonal rod packing. Thermal displacement ellipsoids drawn at 75% probability level. White: C, blue N, red: Se, gray: *A*.

pack in the form of a distorted pseudohexagonal rod packing (see Figure 1c). However, the structural description can be simplified if only the centers of the octahedra, the cation positions, are considered. In this case those form the distorted motif of a hexagonal primitive packing where the $SeCN^-$ anions occupy the trigonal prismatic voids thus forming a distorted variant of the NiAs-type.

### Crystal structure of K[SeCN]

The crystal structure of K[SeCN] has been described previously[5] and was here redetermined with higher precision of lattice parameters, atomic coordinates, interatomic distances and angles. K[SeCN] crystallizes in its own structure type in the monoclinic system with space-group $P2_1/c$ (no. 14, $a=4.4211(9)$, $b=7.502(2)$, $c=11.781(2)$ Å, $\beta=101.63(3)°$), see Table S1 for details on data collection and structure refinement. Phase purity was confirmed by PXRD and subsequent Rietveld refinement confirmed the model within small margins (see Table S3 and Figure S3).

All atoms occupy the general position with Wyckoff symbol 4*e*. The potassium ion is coordinated by seven selenocyanate anions forming a capped trigonal prism (Figure 2a). The four the K–Se distances are in the expected range (3.339(1) to 3.444(1) Å). Two of the three K–N distances are 2.813(3) and 3.010(3) Å which is in the expected range for the sum of their ionic radii, and one distance is considerably larger (3.810(1) Å) leading to (6 + 1) coordination of the potassium ion.

The selenocyanate anions are located in between the potassium ions with each nitrogen terminus connecting to three, each selenium terminus to four other potassium cations. When only the K-N contacts are taken into account, one can construct a ladder of distorted $K_2N_2$ squares ($\sphericalangle_{K\text{-}N\text{-}K}=108.02(9)°$ and $\sphericalangle_{N\text{-}K\text{-}N}=71.98(8)°$, see Figure 2b) which extends along [100]. The rod itself exhibits rod group symmetry $\not{1}_a\,\bar{1}$ (no. 2) and its lattice periodicity is the *a* axis of the parent space-group. Due to space-group symmetry there are two orientations of this ladder and those pack in the type of a distorted hexagonal rod packing (see Figure 2c).

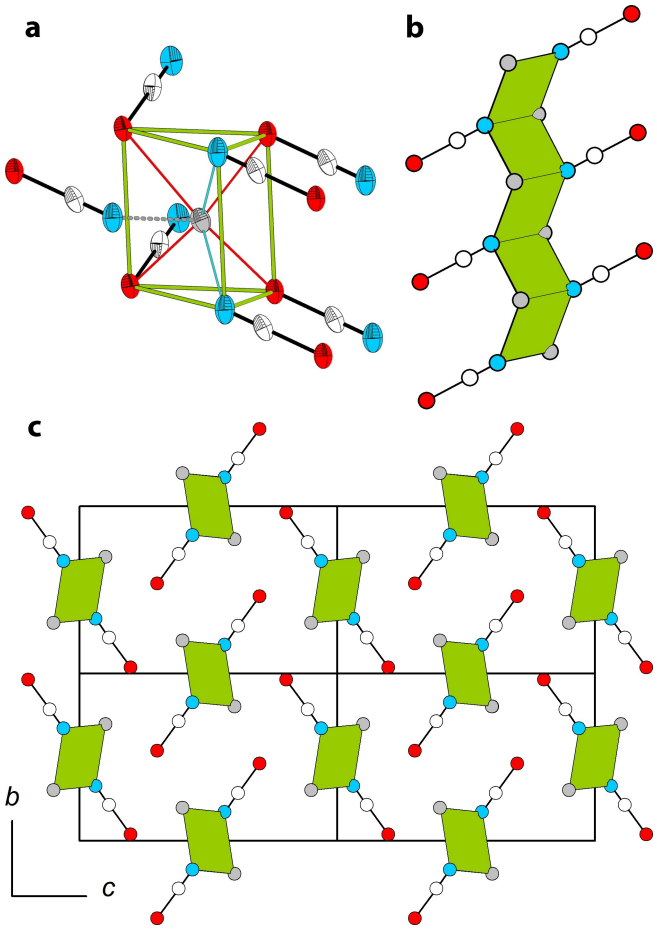


**Figure 2.** The crystal structure of K[SeCN]. a) Coordination around potassium in the form of a capped trigonal prism. b) formation of distorted $K_2N_2$ squares stacked along [100] with rod group symmetry $\not{1}_a\,\bar{1}$. c) 1×2×2 supercell emphasizing the distorted pseudohexagonal rod packing. Thermal displacement ellipsoids drawn at 75% probability level. White: C, blue N, red: Se, gray: *A*.

### Crystal structures of Rb[SeCN] and Cs[SeCN]

Rb[SeCN] and Cs[SeCN] crystallize isotypically in the Cs[SCN]-type in space-group *Pnma* (no. 62, Rb[SeCN]: $a=7.9241(2)$, $b=6.0678(2)$, $c=8.0988(3)$ Å, Cs[SeCN]: $a=8.1188(6)$, $b=6.3387(3)$, $c=8.4813(5)$ Å) with 4 formula units in the unit cell (see Table S1 for details on data collection and structure refinement). Phase purity was confirmed by PXRD and subsequent Rietveld refinement confirmed the model within small margins (see Table S3 and Figure S4 & S5). Cell parameters for Cs[SeCN] have been reported previously, albeit without refined data or a structure model.[13] We were able to confirm the parameters and rule out the suggested space-group type $Pn2_1a$.

The structure consists of layers (see Figure 3d) in the *ab* plane which are stacked along [010]. Each cation is surrounded by four $SeCN^-$ anions from this plane ($d_{(Rb\text{–}N)}=3.005(6)$ and 3.001(5) Å, $d_{(Rb\text{–}Se)}=3.5959(8)$ and 3.6344(8) Å, $d_{(Cs\text{–}N)}=3.176(5)$ and 3.195(5) Å, $d_{(Cs\text{–}Se)}=3.7570(6)$ and 3.7975(6) Å). From the planes above and below four additional $SeCN^-$ anions are in close proximity two of which connect via their selenium terminus ($d_{(Rb\text{–}Se)}=3.7625(5)$ Å and $d_{(Cs\text{–}Se)}=3.9097(4)$ Å) and two via their nitrogen terminus ($d_{(Rb\text{–}N)}=3.274(2)$ Å and $d_{(Cs\text{–}N)}=3.397(2)$ Å). In total this results in a coordination polyhedron with 8 vertices which can be best described as a highly distorted cube (see Figure 3a).

In contrast to *A*[SeCN] (*A* = Li–K) the extended structures of Rb[SeCN] and Cs[SeCN] cannot be rationalized by packing of rods but are better described by the cation positions. In the *ab*-plane the cations form a rectangular motif which is stacked in an A–B–C–D sequence along [001] (see Figure S7). The individual rectangular motifs are then interconnected by selenocyanate ions. The structure is related to the $CsI_3$ type where the cation positions are similar and atoms from the selenocyanate anion occupy halogen atom positions. Here, the nitrogen atom occupies the more ionic position of the unsymmetric $I_3^-$ anion,

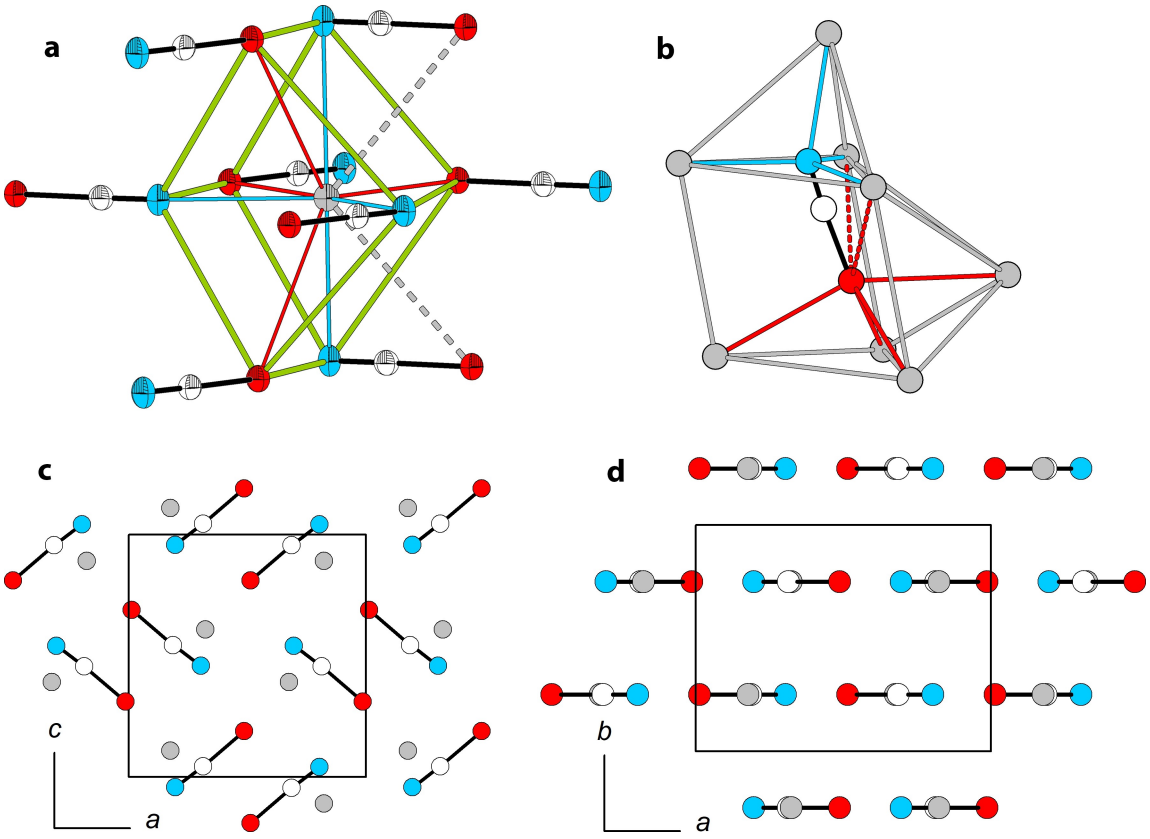


**Figure 3.** Crystal structure of Rb[SeCN] (Cs[SeCN] crystallizes isotypically). a) Coordination around the cation in the form of a severely distorted cube. b) Coordination sphere around the $SeCN^-$ anion. c/d) Extended unit cells viewed along [010] and [001], respectively. Thermal displacement ellipsoids drawn at 75% probability level. White: C, blue N, red: Se, gray: *A*.

evident by the near tetrahedral coordination with four cations in close contact (see Figure 3b). The less ionic C–Se part is surrounded by six cations in total, two of which show long interatomic distances ($d_{(Se–Rb)}$ = 3.9588(5) Å, $d_{(Se–Cs)}$ = 4.0757(4) Å) and are also in the coordination sphere of the N atom.

### Crystal structure of $Li[SeCN]\cdot 2H_2O$

Of all alkali-metal selenocyanates, only Li[SeCN] forms a hydrate. $Li[SeCN]\cdot 2H_2O$ crystallizes isotypical with $Li[SCN]\cdot 2H_2O$[16] in the orthorhombic system with space-group *Pnma* (no. 62, *a* = 5.7131(2), *b* = 8.3814(2), *c* = 9.8823(3) Å) with *Z* = 4 (see Table S2 for details on data collection and structure refinement). Li, N, C, and Se atoms occupy the position with Wyckoff symbol 4*c*, whereas the $H_2O$ molecules occupy the general position 8*d*. Each cation is surrounded by four $H_2O$ molecules ($d_{(Li–O)}$ = 2.116(3) and 2.071(3) Å, see Figure 4a) and two $SeCN^-$ anions which both coordinate via their N-terminus.

However, one anion is significantly farther away ($d_{(Li–N)}$ = 2.871(5) Å) than the other ($d_{(Li–N)}$ = 2.080(5) Å) leading to a 5 + 1 coordination of the cation in the form of a distorted unsymmetrical square bipyramid.

Both the selenocyanate anion and the water molecules serve as bridging ligands connecting the cations into rods with rod-group type $\not{p}_a$ 1 $2_1/m$ 1 that extend along [100] (see Figure 4b). The rods form the motif of a distorted pseudohexagonal rod packing and are themselves interconnected by a Se–H hydrogen bonding network ($d_{(Se–H)}$ = 2.56(2) Å, see Figure 4c). Within the rods there are also weak Se–H hydrogen bonds with d(Se–H) = 2.90(2) Å.

### Geometry of the $SeCN^-$ anion

For all structures discussed here the $SeCN^-$ anion is almost linear with angles 176.7(5)–179.8(1)°. The Se–C bond lengths range from 1.8073(4)–1.8176(1) Å and are longer than the C=Se double bond in $CSe_2$ (1.692(2) Å) and shorter than the C–Se single bond in $Se(Ph)_2$ (1.924(3) Å).[17,18] C–N distances in the $SeCN^-$ anion range from 1.1571(2)–1.1648(2) Å and are thus comparable to a C≡N triple bond (1.16 Å).

### Vibrational spectra

For all quasibinary alkali-metal selenocyanates their structures in the solid state were optimized with the DFT-PBE0-D3 method and IR and Raman spectra were calculated. Experimental structures were reproduced within small margins. The calcu-

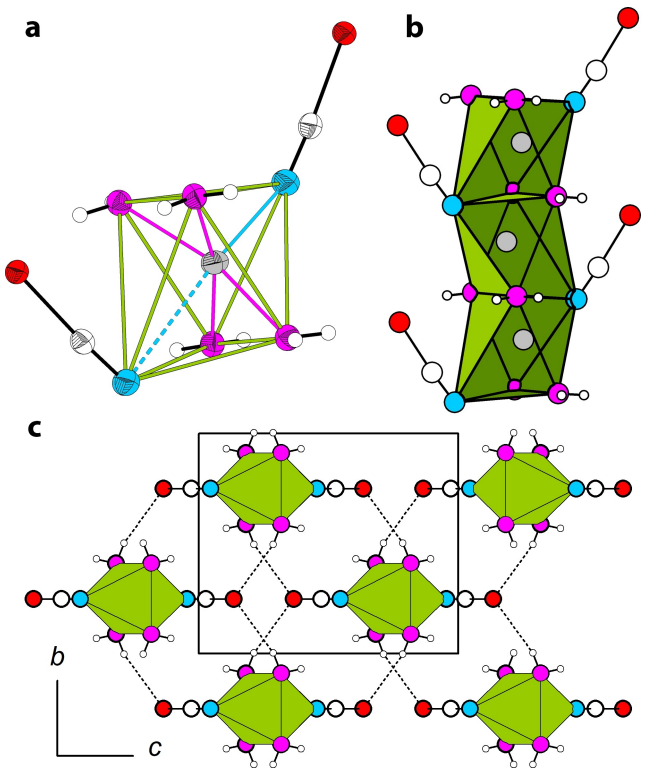


**Figure 4.** Crystal structure of Li[SeCN]·$2H_2O$. a) Coordination around the cation in the form of an unsymmetrical square bipyramid. b) Rod of face sharing polyhedral with rod group symmetry $\not{h}_a 1\ 2_1/m\ 1$. c) Extended unit cell viewed along [100] emphasizing the distorted pseudohexagonal rod packing and the Se–H network (dashed contacts). Thermal displacement ellipsoids drawn at 75% probability level. White: C, blue N, red: Se, magenta: O, small white: H gray: *A*.

lated vibrational frequencies have been obtained within the harmonic approximation and they are systematically overestimated in comparison to the experimental frequencies. Details on methodology, calculated band positions and assignments are given in the Supporting Information.

The IR spectra of all selenocyanates are dominated by the $\nu 1$ ("antisymmetric") stretching mode of the selenocyanate anion (2055–2089 $cm^{-1}$, see Table 1). Only for Li[SeCN] also the $\nu 2$ ("symmetric") stretching mode can be observed at 588 $cm^{-1}$.

**Table 1.** Comparison and assignment of IR-active bands for *A*[SeCN] with *A* = Li–Cs. All values given in $cm^{-1}$, literature value for K[SeCN] given in parentheses.

| Compound | $\nu 1$ stretching | $\nu 2$ stretching | Reference |
|---|---|---|---|
| Li[SeCN] | 2089 | 588 | this work |
| | 2224, 2214 | 638, 632 | DFT-PBE0-D3 |
| Na[SeCN] | 2057 | not obs. | this work |
| | 2232, 2227 | 605, 600 | DFT-PBE0-D3 |
| K[SeCN] | 2069 (2070) | not obs. (558) | this work,[19] |
| | 2202, 2199 | 604, 604 | DFT-PBE0-D3 |
| Rb[SeCN] | 2057 | not obs. | this work |
| | 2181, 2178 | 604, 604 | DFT-PBE0-D3 |
| Cs[SeCN] | 2055 | not obs. | this work |
| | 2189, 2181 | 603, 601 | DFT-PBE0-D3 |

Similarly, the Raman spectra are also dominated by the $\nu 1$ stretching mode of the selenocyanate anion which here are a combination of $B_{3g}$ and $A_g$ modes (2101–2055 $cm^{-1}$, see Table 2). In all cases the $\nu 2$ mode is also observed (571–586 $cm^{-1}$). While the $\delta 1$ rocking mode of $SeCN^-$ calculated for ~450 $cm^{-1}$ is unobserved for all compounds, lattice vibrations can be observed at low wavenumbers for *A*[SeCN] (*A* = Li–Rb) selenocyanates. Lattice vibrations for Cs[SeCN] are out of the range of Raman spectroscopy and calculated to be at 100 $cm^{-1}$.

## Thermal behavior

Melting points for *A*[SeCN] (*A* = Li–Cs) have been obtained by differential scanning calorimetry and thermal gravimetric analysis (DSC-TGA) measurements. Initial experiments with 10 K/min heating rates were conducted from r.t. to 1000 °C to find melting points. Subsequent measurements with 1 K/min heating rates were conducted to accurately determine the melting points, see Table 3.

We were able to reproduce previously reported melting point for Cs[SeCN].[13] Possibly due to the different crystal structures, the melting points do not follow a general trend. However, in the isostructural pairs Li[SeCN]/Na[SeCN] and Rb[SeCN]/Cs[SeCN] the respective heavier homologue exhibits the higher melting point.

For as-synthesized Li[SeCN], the amorphous-to-Crystalline phase transition is a slow process starting at ca. 80 °C which was verified by variable temperature powder X-ray diffraction (VT-PXRD). If stored for prolonged (>6 months) time at ambient temperature, however, samples of Li[SeCN] show broad

**Table 2.** Comparison and assignment of Raman-active bands for *A*[SeCN] with *A* = Li–Cs. All values given in $cm^{-1}$, literature value for K[SeCN] given in parentheses.

| Compound | $\nu 1$ stretching | $\nu 2$ stretching | lattice vibration | Reference |
|---|---|---|---|---|
| LiSeCN] | 2090 | 586 | 150 | this work |
| | 2215, 2204 | 622, 619 | 166, 162 | DFT-PBE0-D3 |
| Na[SeCN] | 2101 | 573 | 148 | this work |
| | 2230, 2224 | 602, 599 | 163, 156 | DFT-PBE0-D3 |
| K[SeCN] | 2074 (2075) | 588 (558) | 160 | this work,[19] |
| | 2205, 2194 | 605, 604 | 172, 166 | DFT-PBE0-D3 |
| Rb[SeCN] | 2064 | 564 | 153 | this work |
| | 2180, 2168 | 605,604 | 161, 150 | DFT-PBE0-D3 |
| Cs[SeCN] | 2057 | 571 | not obs. | this work |
| | 2180, 2172 | 601, 601 | 100 | DFT-PBE0-D3 |

**Table 3.** Melting points (onset) for *A*[SeCN] (*A* = Li–Cs) as measured from DSC-TGA, values in °C. Literature value Cs[SeCN] given in parentheses.

| Li[SeCN][a] | Na[SeCN] | K[SeCN] | Rb[SeCN] | Cs[SeCN] |
|---|---|---|---|---|
| 212 | 273 | 155 | 133 | 224 (228) |

[a] The amorphous-to-Crystalline phase transition starts at ca. 80 °C.

reflections (marked with asterisk in Figure 5) which do not coincide with reflections for the *Pnma*-phase. The DSC-TGA data also shows additional features at 115 and 154 °C. VT-PXRD showed that upon heating to 80 °C the expected reflections for the structural model in *Pnma* appear and the broad reflections gradually disappear and are fully absent at T > 160 °C. The DSC-signal at 115 °C does not coincide with changes in the PXRD pattern. Thus, we attribute the reflections to a still unknown modification of Li[SeCN] the structure of which we were unable to obtain thus far. Additionally, the molten Li[SeCN] shows a rather high vapor pressure as evident by the constant mass-loss observed in the TGA. If heated above the melting point in a sealed capillary as used for PXRD measurements, the increased pressure led to the bursting of the capillary around ca. 300 °C.

## Conclusion

*A*[SeCN] (*A* = Li–Rb) were prepared by oxidation of the respective cyanides with selenium either mechanochemically (Li[SeCN]) or in solution (*A* = Na–Rb). Cs[SeCN] was prepared by metathesis starting from CsCl and K[SeCN]. The coordination numbers of the cations in the solid state increase with increasing ionic radius from Li[SeCN]/Na[SeCN] (CN = 6), over K[SeCN] (CN = 6 + 1) to Rb[SeCN]/Cs[SeCN] (CN = 8). Their crystal structures can be rationalized by distorted hexagonal rod packings (for Li[SeCN]/Na[SeCN] and K[SeCN]). In contrast, Rb[SeCN]/Cs[SeCN] form a layered structure. Solely lithium selenocyanate forms a hydrate with the formula Li[SeCN]·2$H_2O$. Quantum chemical calculations of *A*[SeCN] allowed for complete assignment of the recorded solid-state vibration spectra which are dominated by the $\nu$1 ("antisymmetric") stretching mode of the selenocyanate anion. Melting points were extracted from DSC-TGA data. Amorphous as-synthesized Li[SeCN] stored for > 6 months shows broad reflections indicative for a possibly metastable polymorph, which is currently under investigation.

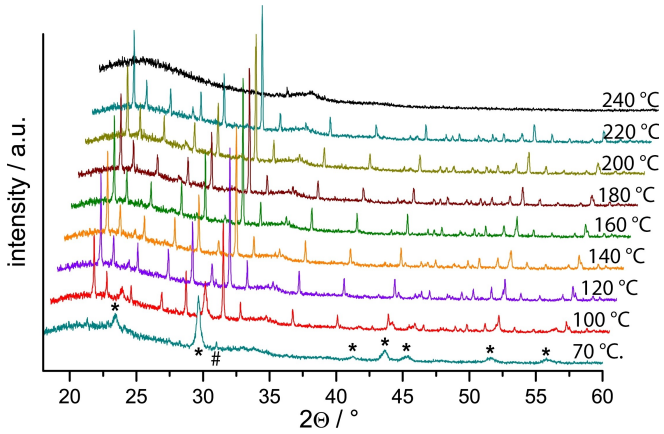


**Figure 5.** PXRD patterns of Li[SeCN] at 70 °C (front) and from 100 °C to 240 °C (back) in 20 K increments. * marks reflections of the proposed metastable phase, # the strongest reflection for the *Pnma* phase.

## Experimental Section

Experimental details, tables for SCXRD and PXRD data incl. refinements, Raman and IR spectra, computational data, and DSC-TGA data can be found in the Supporting Information.

**Crystal structure analysis**: Deposition Numbers 2080507 (for Li[SeCN]), 2080515 (for Na[SeCN]), 2080510 (for K[SeCN]), 2080509 (for Rb[SeCN]), 2080514 (for Cs[SeCN]), 2080516 (for [Li@12-crown-4][SeCN]), 2080518 (for [Li(MeCN)3SeCN]), and 2080517 (for Li[SeCN]·2H2O) contain the supplementary crystallographic data for this paper. These data are provided free of charge by the joint Cambridge Crystallographic Data Centre and Fachinformationszentrum Karlsruhe Access Structures service.

## *Acknowledgements*

F.T. thanks the Fonds der Chemischen Industrie for a Liebig fellowship. F.T. thanks Prof. Dehnen for excellent support, Prof. Müller and Prof. Kraus for discussions on the crystal structures. Dr. Radostan Riedel is gratefully acknowledged for measuring the single crystal dataset of Na[SeCN]. Jonathan Pfeiffer is gratefully acknowledged for measuring the Raman data. Open access funding enabled and organized by Projekt DEAL.

## Conflict of Interest

The authors declare no conflict of interest.

**Keywords:** alkali-metals · crystallography · selenocyanates · solid-phase synthesis · vibrational spectroscopy

[1] J. J. Berzelius, *Jahresber.* **1822**, *1*, 49.
[2] A. Wiggers, *Ann. der Pharm.* **1839**, *29*, 319–319.
[3] K. Huttner, S. Knappe, *Z. Anorg. Allg. Chem.* **1930**, *190*, 27–37.
[4] W. Muthmann, E. Schröder, *Ber. Dtsch. Chem. Ges.* **1900**, *33*, 1765–1769.
[5] D. D. Swank, R. D. Willett, *Inorg. Chem.* **1965**, *4*, 499–501.
[6] A. W. Downs, *Chem. Commun.* **1968**, 1290–1291.
[7] A. S. Foust, *J. Chem. Soc. Chem. Commun.* **1979**, 414–415.
[8] A. H. Norbury, *Adv. Inorg. Chem. Radiochem.* **1975**, *17*, 231–386.
[9] J. Fonseca, T. Gong, L. Jiao, H. L. Jiang, *J. Mater. Chem. A* **2021**, *9*, 10562–10611.
[10] S. Roy, A. Dey, P. P. Ray, J. Ortega-Castro, A. Frontera, S. Chattopadhyay, *Chem. Commun.* **2015**, *51*, 12974–12976.
[11] R. Neri, S. H. Bossmann, *Synth.* **2021**, *53*, 2015–2028.
[12] L. Birckenbach, K. Kellermann, *Ber. Dtsch. Chem. Ges.* **1925**, *58*, 2377–2386.
[13] S. Hauge, *Acta Chem. Scand.* **1971**, *25*, 3081–3093.
[14] G. A. Bowmaker, A. V. Churakov, R. K. Harris, J. A. K. Howard, D. C. Apperley, *Inorg. Chem.* **1998**, *37*, 1734–1743.
[15] L. Birckenbach, K. Kellermann, *Ber. Dtsch. Chem. Ges.* **1925**, *58*, 786–794.
[16] O. Reckeweg, A. Schulz, B. Blaschkowski, T. Schleid, F. J. DiSalvo, *Z. Naturforsch. B* **2014**, *69*, 17–24.
[17] S. Bhandary, A. Sirohiwal, R. Kadu, S. Kumar, D. Chopra, *Cryst. Growth Des.* **2018**, *18*, 3734–3739.
[18] A. G. Maki, R. L. Sams, *J. Mol. Spectrosc.* **1981**, *90*, 215–221.
[19] H. W. Morgan, *J. Inorg. Nucl. Chem.* **1961**, *16*, 367–370.

Manuscript received: June 10, 2021
Accepted manuscript online: July 16, 2021
Version of record online: August 19, 2021